

From Flutter to Tumble: Inertial Drag and Froude Similarity in Falling Paper

Andrew Belmonte,¹ Hagai Eisenberg,² and Elisha Moses²

¹*Department of Physics and Astronomy, University of Pittsburgh, Pittsburgh, Pennsylvania 15260*

²*Department of Physics of Complex Systems, Weizmann Institute of Science, Rehovot 76100, Israel*

(Received 28 October 1997)

In an experiment on thin flat strips falling through a fluid in a vertical cell, two fundamental motions are observed: side-to-side oscillation (flutter) and end-over-end rotation (tumble). At high Reynolds number, the dimensionless similarity variable describing the dynamics is the Froude number Fr , being the ratio of characteristic times for downward motion and pendular oscillations. The transition from flutter to tumble occurs at $Fr_c = 0.67 \pm 0.05$. We propose a phenomenological model including inertial drag and lift which reproduces this motion, and directly yields the Froude similarity. [S0031-9007(98)06387-X]

PACS numbers: 47.27.Vf, 03.40.Gc

Not all falling objects travel straight downwards: a piece of paper dropped from the table or a leaf as it flutters to the ground are two common examples. This is due primarily to the coupling of forward motion to lateral oscillations by the surrounding fluid [1–3]. The resulting dynamics are relevant to systems ranging from aircraft stability [3,4] to rising bubbles [5]. The problem of falling paper is rich in hydrodynamic effects, including lift, drag, vortex shedding, and stall, and has a history dating back to Maxwell, who noticed in 1854 that the combination of gravity and lift results in a torque [6]. Despite subsequent theoretical work by Helmholtz, Kelvin, and others [1,3], including a formal irrotational analysis due to Kirchhoff [1], a solution of the complete problem is impractical, and the correct description remains undetermined. This extensive theoretical background has not been matched experimentally. Previous falling object experiments have been fully three dimensional [7–11], reporting fluttering, gyrating, or tumbling, but few quantitative specifics of the dynamics were given. While it is clear that vortices are shed simultaneous to the oscillations, it is unknown if the vortices result from or cause the oscillations [12,13].

More recently, phenomenological models have successfully elicited qualitative aspects of the motion [14–18], although with some debate on the role of viscosity and the existence of chaotic tumbling. However, these models either ignore the vortices by treating the flow as irrotational, or assume a viscous drag, or omit drag altogether. Surprisingly, in almost 150 years, there is no experimentally verified description for this rather basic phenomenon.

We present here a simple laboratory experiment on flat strips dropped in a quasi-2D geometry [19]. Our experimental cell is a narrow fluid-filled glass aquarium, 60 cm in height and length and 0.8 cm wide, into which thin strips made of various materials are dropped. The strips are constructed of plastic, brass, or steel, each with about the same thickness (0.1–0.2 cm) and width (0.75 cm), but with a range of lengths L . Using different materials allows us to vary L and the mass M independently, from

1 to 32 cm and 1 to 7 g, respectively. We use three different fluids: water, a glycerol/water mixture (40:60 by weight), and petroleum ether, with densities ρ of 1.00, 1.10, and 0.67 g/cm³, and viscosities of 0.010, 0.036, and 0.003 P, respectively. Two thin stabilizing rings attached to each side (typically of 1 mm diameter steel wire; see inset of Fig. 2) keep the strip from turning over in the third (narrow) dimension. The ring radius R is chosen so that its main effect is to increase the total mass [20]. Grazing or sticking to the wall is rarely seen due to lubrication layer effects. The motion of the strip is imaged with a video camera, and recorded for later analysis.

We observe two fundamental motions: side-to-side oscillation (flutter) and end-over-end rotation (tumble), shown in Fig. 1. By digitizing every frame, we obtain the strip position vs time; the stabilizing rings are black and therefore not visible. In Fig. 2a we show the time variation of the angle Θ that the strip makes with the horizontal (see inset); it ranges between $\pm\Theta_{\max}$. The vertical velocity V_y reaches its maximal downward value as Θ approaches Θ_{\max} (Fig. 2b), corresponding to the

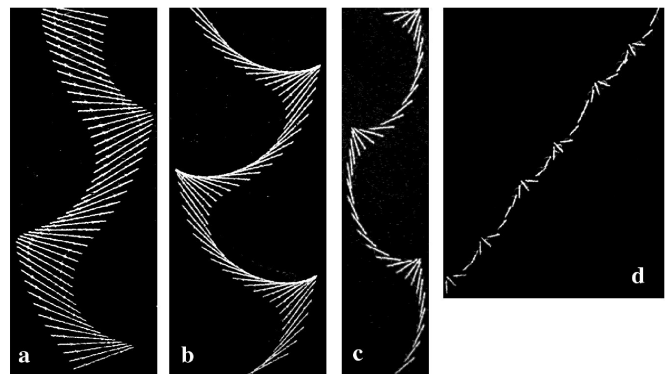


FIG. 1. Collage of consecutive video fields ($\Delta t = 0.02$ sec) for strips falling in water: (a) $L = 5.1$ cm, $M = 2.9$ g ($Fr = 0.37$); (b) $L = 4.1$ cm, $M = 2.7$ g ($Fr = 0.45$); (c) $L = 2.0$ cm, $M = 1.4$ g ($Fr = 0.65$); (d) $L = 1.0$ cm, $M = 0.7$ g ($Fr = 0.89$).

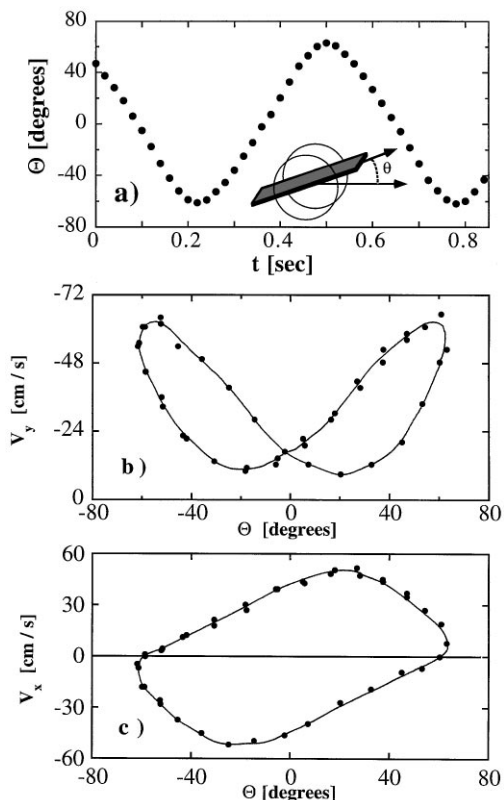


FIG. 2. Measured dynamics of a falling strip ($M = 2.0$ g, $L = 3.0$ cm, $Fr = 0.53$). (a) Angle Θ vs time. The inset shows the strip, the stabilizing rings and the angle Θ . (b) Vertical velocity V_y vs Θ . (c) Horizontal velocity V_x vs Θ .

minimal drag of a small “angle of attack” [4]. As Θ decreases so does V_y , which reaches its minimum not at $\Theta = 0$, when the strip faces broadside into the flow, but at $\Theta \approx 20^\circ$. A similar effect was observed in the pioneering work of Eiffel [21]. The butterfly shape in Fig. 2b indicates that V_y oscillates at half the period of Θ . The horizontal velocity V_x oscillates around zero with the same period as Θ (Fig. 2c); at $\Theta \approx 20^\circ$ V_x is maximum.

This description applies to all strips with $\Theta_{max} < 90^\circ$. Beyond this value the strip tumbles end over end (Fig. 1d). We therefore use Θ_{max} as the order parameter for this transition. We then find that the control parameter is given by the ratio of characteristic times for the downward fall and the rotational flutter. For large enough velocities, the terminal downward velocity is determined by gravity and the “form” or inertial drag $F_d = C\rho V^2 S$ [21], where S is the cross-sectional area of the object, V is the velocity, and C is a constant of the order of 1. For our strips the terminal velocity scale is $U_0 = (M'g/\rho Lw)^{1/2}$, where M' is the buoyancy corrected mass and w is the width of the strip [22]. The downward motion is characterized by the time scale $\tau_v = L/U_0$. The pendular motion of fluttering is characterized by the time scale of a buoyant pendulum: $\tau_p = (ML/M'g)^{1/2}$. The ratio of the two time scales is the Froude number

$$Fr = \frac{\tau_p}{\tau_v} = \frac{U_0}{(M'gL/M)^{1/2}} = \left(\frac{M}{\rho L^2 w}\right)^{1/2}. \quad (1)$$

In our experiments Fr varies from 0.02 to 1.0. A plot of $\sin(\Theta_{max})$ vs Fr is shown in Fig. 3a; all data collapse onto a single curve given by $\sin(\Theta_{max}) = (1.50 \pm 0.03)Fr$. The three fluids used differ in viscosity (factor of 10) and density (factor of 0.6), but only the density as included in Eq. (1) could account for the changes in $\sin(\Theta_{max})$. The tumbling transition [$\sin(\Theta_{max}) > 1$] occurs at a value of $Fr_c = 0.67 \pm 0.05$. This corresponds to a pendulum driven at resonance: $\tau_v \approx \tau_p$ ($Fr \approx 1$) [23].

In general, the motion of the strips should also depend on the Reynolds number $Re = \rho UL/\eta$, which for our experiments ranges from about 3×10^3 to 4×10^4 . Our scaling in terms of Fr , however, shows that the fluttering is independent of viscosity. This result is in agreement with previous observations that, for high enough Re , the motion is Re independent [7,13].

The role that Fr plays in our analysis is common to systems which are controlled by the competition of a speed of propagation and a dissipative speed [24], and in our case it provides a physically relevant equivalent to the scaling first implied in [7]. It was first defined by Froude in 1874 as the similarity variable for surface ships [1,25,26], being the ratio of ship to wave speed. A more surprising example

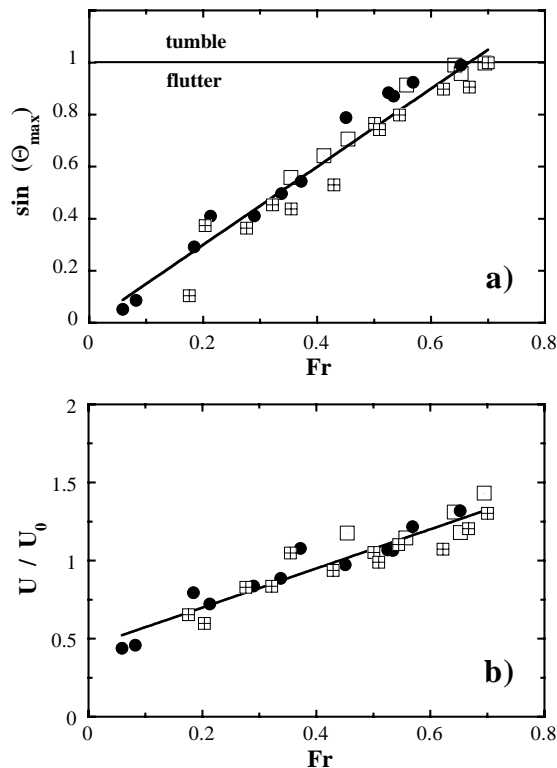


FIG. 3. (a) The order parameter $\sin(\Theta_{max})$ vs the control parameter Fr . (b) The velocity ratio U/U_0 vs Fr . Fluids are water (circles), petroleum ether (open squares), and water/glycerol (crossed squares). The straight lines are linear fits.

of Fr similarity is the pendulum model of walking, which accounts for the exchange between gravitational potential and swinging kinetic energy of the leg during a forward stride [24]. The comparative analysis of gait for a wide variety of animals [26,27] shows that the transition from walking to running in bipeds, or to trotting in quadrupeds, occurs at $Fr_c \approx 0.8$ [27].

To verify our Fr scaling, we measure the average vertical downwards velocity: $U \equiv -\langle V_y \rangle$. Plotting U/U_0 vs Fr in Fig. 3b, we find that all points fall onto a single curve, given by $U/U_0 = (1.25 \pm 0.09)Fr + (0.45 \pm 0.04)$. Note that $U \approx U_0$ over the range of Fr in our experiment.

For strips with $Fr > Fr_c$, we observe a continuous tumbling rotation; for values just above Fr_c we also sometimes observe random reversals of the rotation direction, similar to what is observed in simulations [15,16]. However, the length of the trajectories is insufficient to determine if they are strictly chaotic [11].

We also directly measure the parallel (F_{\parallel}) and perpendicular (F_{\perp}) drag force by towing the strips in each direction with a known force, while restraining the fluttering. The drag force is indeed quadratic in velocity [21]: $F_{\parallel} = -A_{\parallel}\rho wLV^2$ and $F_{\perp} = -A_{\perp}\rho wLV^2$, with $A_{\perp} = 4.1 \pm 0.1$ and $A_{\parallel} = 0.88 \pm 0.03$. Our experimental conclusion that the relevant drag force is quadratic and not linear in velocity constitutes a fundamental departure from existent models, in which drag terms originate from either viscosity [16] or an irrotational representation [1,18].

We therefore modify the model in [16] to include only lift, gravity, and *inertial* drag. Although added mass effects are surely present [1,15,18], our experiments indicate that they are not significant. The drag parallel and perpendicular to the strip is $F_{\parallel} = -A_{\parallel}\rho wLV^2 \cos(\gamma - \Theta)$ and $F_{\perp} = -A_{\perp}\rho wLV^2 \sin(\gamma - \Theta)$, where γ is the angle of the velocity vector (V_x, V_y) from the positive x axis, and $V^2 = V_x^2 + V_y^2$. The rotational drag is $F_{\omega} = -A_{\omega}\rho wL^4\omega^2$, where ω is the angular velocity. These replace the viscous forces in [16]; the lift force is the steady state value given by the Kutta-Joukowski theorem [1,4,16], where the circulation depends on the velocity, and thus can vary. From our simulations we choose $A_{\omega} = 0.0674$, which fixes the tumbling transition at $Fr_c = 0.67$.

Using U_0 and τ_p to nondimensionalize our model, and writing $\phi = \gamma - \Theta$, the equations are

$$\begin{aligned} \dot{V}_x &= \frac{V^2}{Fr} \left[A_{\perp} \sin \phi \sin \Theta - A_{\parallel} \cos \phi \cos \Theta \right. \\ &\quad \left. + 4\pi |\sin \phi| \cos \left(\gamma \pm \frac{\pi}{2} \right) \right] \\ \dot{V}_y &= -\frac{V^2}{Fr} \left[A_{\perp} \sin \phi \cos \Theta + A_{\parallel} \cos \phi \sin \Theta \right. \\ &\quad \left. - 4\pi |\sin \phi| \sin \left(\gamma \pm \frac{\pi}{2} \right) \right] - \frac{1}{Fr} \end{aligned}$$

$$\dot{\omega} = \pm A_{\omega} \frac{12\omega^2}{Fr^2} - 6\pi V^2 \sin(2\phi); \quad \dot{\Theta} = \omega.$$

Note that the Fr scaling is clearly evident in the equations; this arises from the dependence of both lift and drag on V^2 . The sign conventions ensure that the strip is always inside the right angle formed by the lift and velocity vectors, and that rotation by π does not change the equations. We emphasize that our equations are not a particular case of the potential flow solutions to Laplace's equation [1,18], but the result of including the effects of vortex shedding via inertial drag and variable circulation.

Employing a standard Runge-Kutta integration scheme, we obtain trajectories that are very close to the experimental ones, as shown in Fig. 4 for the parameters of Fig. 1b [28]. Just near Fr_c the model exhibits additional frequencies and apparent chaotic behavior, similar to existing models [14–17]; these are not observed experimentally. The coefficient A_{ω} affects not only the value of Fr_c but also the smoothness of the curves; small differences in A_{ω} may explain qualitative differences in the trajectories (Fig. 1a–1c). A detailed comparison of the experimental and numerical trajectories shows that the model reproduces the fluttering dynamics extremely well. A slight deviation does occur at the turning points, where Θ changes rapidly. This tendency towards apparently singular behavior grows inversely with A_{ω} , and must also depend on the magnitude of the lift coefficients. This effect points to the necessity of explicitly treating the vortex shed at each turning point, for example, by including another differential equation for the lift [12].

What are the dynamics of the surrounding fluid? The falling strip creates a zigzag wake by shedding vortices synchronized with its fluttering oscillations, as shown by alumina particle visualization in Fig. 5. A small whirl develops behind the side which is swinging upwards, and is shed when the angle reaches Θ_{\max} . This attached vortex may be a major factor in stabilizing the moment driving rotation [13], and may also modify the lift [29]. An oscillating lift could drive the fluttering motion, since

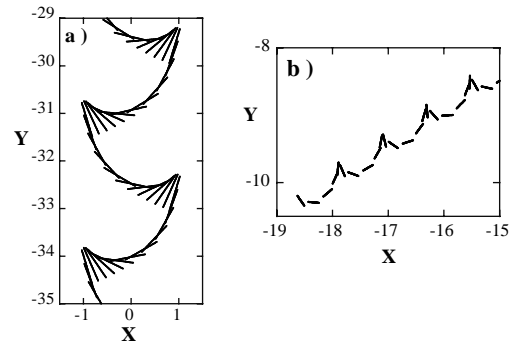


FIG. 4. Two collages of the simulation (see [28]), with Fr corresponding to the data in Figs. 1(b) and 1(d). The strips are shown every $\Delta t = 0.4\tau_p$: (a) $Fr = 0.45$, $L = 0.75$ (flutter); (b) $Fr = 0.89$, $L = 0.19$ (tumble).

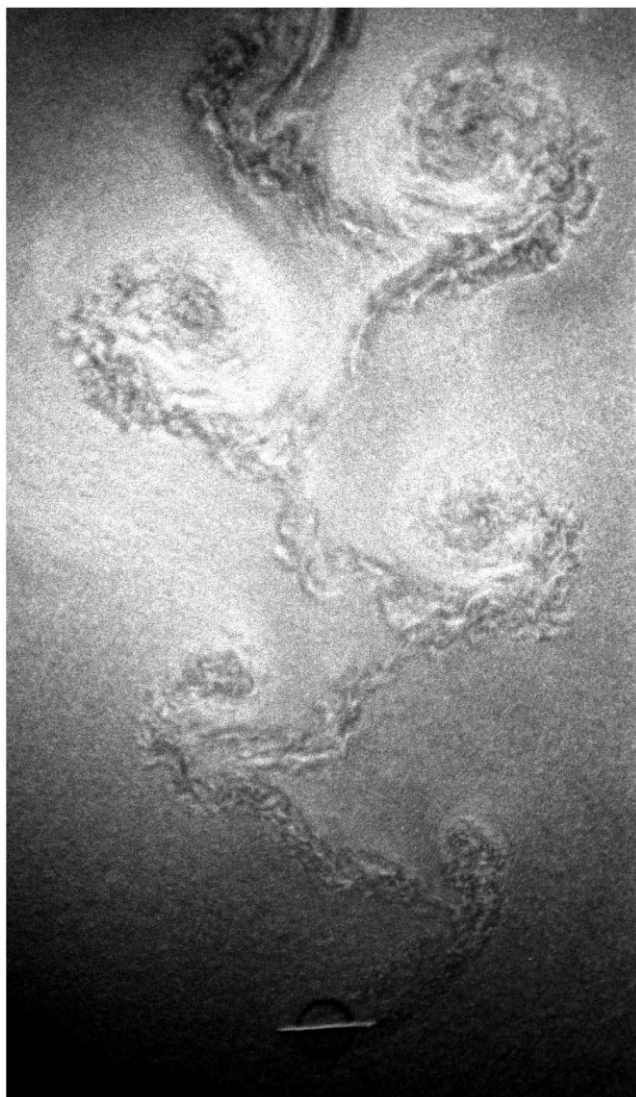


FIG. 5. Aluminum particle visualization of the flow behind a fluttering strip: $L = 4.1$ cm, $M = 2.7$ g ($Fr = 0.45$).

vortex shedding produces an oscillating side thrust [12]. A full treatment of these effects is lacking in our analysis.

Our experiment has shown that the transition from flutter to tumble is determined by the Froude number, with a velocity scale set by the inertial drag. The model motivated by these observations reproduces this transition, and implies the Fr similarity. The vortices and the high Re flow around the strip are responsible for the inertial drag, although they do not appear dynamically in our model. Nonetheless, Fr adequately describes the gross features of the motion. What remains experimentally is to explore *quantitatively* the attached vortex, the lift dynamics during flutter, and the dynamics of tumble.

We thank J. Fineberg, L. Mahadevan, H. Stone, R. Zeitak, and O. Zik for discussions. A.B. acknowledges support from the NSF and a NASA Research Grant.

This work was supported by the Minerva Foundation, Munich, and the Minerva Center for Nonlinear Physics.

-
- [1] H. Lamb, *Hydrodynamics* (Dover, New York, 1945), 6th ed.
 - [2] M. J. Lighthill, *Annu. Rev. Fluid Mech.* **1**, 413 (1969).
 - [3] H. J. Lugt, *Annu. Rev. Fluid Mech.* **15**, 123 (1983).
 - [4] R. von Mises, *Theory of Flight* (McGraw-Hill, New York, 1945).
 - [5] E. Kelley and M. Wu, *Phys. Rev. Lett.* **79**, 1265 (1997).
 - [6] J. C. Maxwell, in *The Scientific Papers of James Clerk Maxwell* (Dover, New York, 1890), pp. 115–118.
 - [7] W. Willmarth, N. Hawk, and R. Harvey, *Phys. Fluids* **7**, 197 (1964).
 - [8] E. H. Smith, *J. Fluid Mech.* **50**, 513 (1971).
 - [9] R. E. Stewart and R. List, *Phys. Fluids* **26**, 920 (1983).
 - [10] E. Tränkle and M. Riikonen, *Appl. Opt.* **35**, 4871 (1996).
 - [11] S. Field, M. Klaus, M. Moore, and F. Nori, *Nature (London)* **388**, 252 (1997).
 - [12] T. Sarpkaya, *J. Appl. Mech.* **46**, 241 (1979).
 - [13] H. J. Lugt, *J. Fluid Mech.* **99**, 817 (1980).
 - [14] V. V. Kozlov, *Izv. Akad. Nauk SSSR Mekh. Tverd. Tela* **24**, 10 (1989).
 - [15] H. Aref and S. W. Jones, *Phys. Fluids A* **5**, 3026 (1993).
 - [16] Y. Tanabe and K. Kaneko, *Phys. Rev. Lett.* **73**, 1372 (1994); *Phys. Rev. Lett.* **75**, 1421 (1995).
 - [17] L. Mahadevan, H. Aref, and S. W. Jones, *Phys. Rev. Lett.* **75**, 1420 (1995).
 - [18] L. Mahadevan, *C. R. Acad. Sci. (Paris)* **323**, 729 (1996).
 - [19] A. Belmonte, H. Eisenberg, and E. Moses, *Bull. Am. Phys. Soc.* **41**, 1731 (1996).
 - [20] Using $I_{\text{strip}} = ML^2/12$ and $I_{\text{ring}} = mR^2$, the radius is calculated by setting $I_{\text{strip}}/M = I_{\text{ring}}/m$, which yields $R = L/\sqrt{12}$. Thus $I_{\text{tot}} = \frac{1}{12}(M + m)L^2$.
 - [21] G. Eiffel, *La Résistance de l'Air et l'Aviation* (Dunod, Paris, 1911).
 - [22] Since the width of the strips w is always close to the width of the cell, we use $w = 0.8$ cm in our calculations.
 - [23] The geometric asymmetry condition derived via a linear stability analysis in [18] is an equivalent condition.
 - [24] D. W. Thompson, *On Growth and Form* (Cambridge University Press, Cambridge, England, 1942), Chap. 2.
 - [25] W. Froude, *Trans. Inst. Naval Arch.* **11**, 80 (1874).
 - [26] S. Vogel, *Life's Devices* (Princeton University Press, Princeton, NJ, 1988).
 - [27] R. M. Alexander, *Nature (London)* **261**, 129 (1976); *Am. Sci.* **72**, 348 (1984).
 - [28] We determine the length L using the experimentally measured distance that a strip falls in one oscillation. Then for the other strips we use $L_1/L_2 = (Fr_2/Fr_1)^2$.
 - [29] P. G. Saffman and J. S. Sheffield, *Stud. Appl. Math.* **57**, 107 (1977).